Main text word count: 6204

Word count Introduction: 1333

Word count Materials and Methods: 1729

Word count Results: 1098

Word count Discussion: 2044

Number of figures: 6

Colour figures: 6

Number of tables: 1

Supporting information: 6

Title

Wood formation in an evergreen conifer is controlled by phloem transport of labile carbon, but nonstructural carbon concentrations are not

Authors

Tim Rademacher[1,2,3,*], Patrick Fonti[4], James M. LeMoine[1,2], Marina V. Fonti[4,5], David Basler[3], Yizhao Chen[6], Andrew D. Friend[6], Bijan Seyednasrollah[1,2], Annemarie H. Eckes-Shephard[6], and Andrew D. Richardson[1,2]

Addresses

[*] Corresponding author

[1] School of Informatics, Computing, and Cyber Security, Northern Arizona University, Flagstaff, United States

[2] Center for Ecosystem Science and Society, Northern Arizona University, Flagstaff, United States

[3] Department of Organismic and Evolutionary Biology, Harvard University, Cambridge, United States

[4] Swiss Federal Research Institute for Forest, Snow and Landscape Research WSL, Birmensdorf, Switzerland

[5] Institute of Ecology and Geography, Siberian Federal University, Krasnoyarsk, Russian Federation

[6] Department of Geography, University of Cambridge, Cambridge, United Kingdom

Summary

Wood formation is a crucial process for carbon sequestration on land, yet how variations in phloem-transported carbon affect wood formation, respiration and nonstructural carbon pools remains poorly understood.

To better understand the role of carbon supply on allocation to wood formation, we constrained phloem transport using girdling and compression around the stem of 40 mature white pines to monitor the effects of contrasting carbon supply (enriched above and reduced below the manipulations) on local wood formation and respiration, as well as on nonstructural carbon pools in needles, stems, and roots.

Radial growth and respiration responded to variations in carbon supply. Despite a two-fold difference in the number of tracheids formed above and below the manipulation, cell-wall area only decreased slightly and cell size did not change noticeably. Surprisingly, nonstructural carbon pools and concentrations in the xylem, needles and roots remained largely unchanged, although starch reserves were remobilised and accumulated slightly under the most extreme decreases or increases in carbon supply, respectively.

We conclude that phloem carbon supply does not affect nonstructural carbon concentrations but regulates growth and respiration in mature white pine. Thus, wood formation is controlled by the availability of phloem-transported carbon over timescales of several months.

Keywords: Allocation, carbon, growth, nonstructural carbon, respiration, wood anatomy, wood formation, xylogenesis.

1. Introduction

Forests sequester about 26% of anthropogenic carbon emissions each year (Pan *et al.*, 2011) and wood formation is the pivotal process sequestering this carbon for extended periods. Since wood can persist for millennia and is composed of roughly 50% carbon (Lamlom & Savidge, 2003), allocation to wood formation is a salient carbon sink. Understanding the mechanisms of wood formation is therefore crucial to assess land carbon

sequestration in a rapidly changing world (Hartmann *et al.*, 2020) and for accurate predictions of the land carbon cycle (Friend *et al.*, 2019).

Many studies have focused on assessing the "fate" of assimilated carbon in land plants (Atkin, 2015; Hartmann *et al.*, 2020) with the expectation of a direct link between carbon assimilation and fixation into wood structure. Experiments manipulating carbon assimilation by artificially increasing atmospheric CO_2 (Norby & Zak, 2011), defoliating (e.g., Hoch, 2005) or shading trees (e.g., O'Brien *et al.*, 2014) have been often undertaken to describe and quantify the relation between sources and sinks. Growth sinks and carbon status have been shown to be coupled under low atmospheric CO_2 (Hartmann *et al.*, 2013), severe shading (Weber *et al.*, 2019), and defoliation (Piper *et al.*, 2015; Wiley *et al.*, 2017; Fierravanti *et al.*, 2019; Castagneri *et al.*, 2020). However, under increased assimilation due to elevated atmospheric CO_2, plant growth does not increase proportionally to carbon uptake (Ainsworth & Long, 2005). Evidence from tree rings of naturally growing trees suggests a declining response to increasing CO_2 with age (Voelker *et al.*, 2006) or no response at all (van der Sleen *et al.*, 2015), which has also been reported in one CO_2 enrichment study on mature trees (Körner *et al.*, 2005). The comparatively small stimulation of growth may be caused by small trees being more carbon-limited (Körner, 2003; Hayat *et al.*, 2017) due to ontological differences in carbon allocation (Hartmann *et al.*, 2018). This decoupling of carbon assimilation (e.g., photosynthesis) and fixation (e.g., wood formation) has been hypothesised to be the cause of the discrepancy in carbon uptake and growth responses (Fatichi *et al.*, 2014). There is increasing evidence to support that cambial activity is differently and more sensitive to environmental conditions than photosynthesis (e.g., Fromm, 2010; Cabon *et al.*, 2020; Vieira *et al.*, 2020). Environmental sensitivities further complicate the investigation of carbon supply variations on wood formation. Yet, cell division, enlargement and cell-wall deposition have been shown to be affected by changes in the carbon status due to natural defoliation (see Rossi *et al.*, 2009; Deslauriers *et al.*, 2016 for small trees and Castagneri *et al.*, 2020 for larger trees). Thus, despite these great efforts to quantify the relation between assimilation and growth, the debate on what drives allocation to wood formation is not yet settled (Gessler & Grossiord, 2019).

Providing a quantitative *in situ* response of the constituent processes of wood formation (i.e., cell division, cell enlargement and cell-wall deposition) across a gradient of carbon supply should help to disentangle the processes acting along the long pathways between carbon assimilation and fixation in mature trees. Focusing the attention on stem cambial areas, where carbon is permanently fixed into woody structure, reduces complexity such as potentially confounding whole-tree feedbacks. Locally, there are three main carbon sinks in stems: growth, stem respiration and nonstructural carbon pools. Radial growth has been repeatedly inferred to be driven by carbon supply in previous phloem transport manipulations (Wilson, 1968; Maier *et al.*, 2010; Maunoury-Danger *et al.*, 2010; De Schepper *et al.*, 2011), suggesting that wood formation is generally carbon-limited. Stem respiration has been documented to covary with growth along carbon supply gradients (Daudet, 2004; Maunoury-Danger *et al.*, 2010), although questions remain whether observed changes in respiration reflect exclusively changes in energy demand due to variations in growth or partially constitute wound responses (Rademacher *et al.*, 2019). Finally, nonstructural carbon constitutes reserves, that can be remobilised to fuel metabolism in times of scarcity (Carbone *et al.*, 2013; Muhr *et al.*, 2018). Isotopic evidence suggests that growth mainly relied on more recent assimilates, while stem respiration was preferentially fueled by local reserves (Maunoury-Danger *et al.*, 2010). When carbon supply is limited using low atmospheric CO_2 (Hartmann *et al.*, 2015; Huang *et al.*, 2019), drought (Hagedorn *et al.*, 2016), girdling (Regier *et al.*, 2010; Oberhuber *et al.*, 2017) or defoliation (Li *et al.*, 2002; Wiley *et al.*, 2013) observations indicate that allocation to nonstructural carbon reserves is prioritised over growth. On the other hand, little is known about allocation to storage under enhanced carbon supply. At the whole-tree level, we do know that foliage sugar and even more so starch concentrations increase with elevated atmospheric CO_2 (Ainsworth & Long, 2005; Körner *et al.*, 2005; Dawes *et al.*, 2013; but see Schmid *et al.*, 2017), whereas girdling increased local starch concentrations without affecting foliage sugar or starch concentrations (Regier *et al.*, 2010).

In addition to providing local reserves, osmotically active sugars influence turgor pressure (Hölttä *et al.*, 2010; Guerriero *et al.*, 2014). The manipulation of osmotically active sugar concentrations has been suggested to be mainly responsible for changes in growth of girdled

trees (De Schepper & Steppe, 2011). Sugars might also be directly involved in signalling for wood formation, as sugar availability controls the expression of cellular synthesis enzymes and thus play a major role in growth (Riou-Khamlichi *et al.*, 2000). For example, seasonal variations of soluble sugar concentration in the cambium have been hypothesised to be a primary control of intra-annual gradients in cell size and cell-wall thickness (Cartenì *et al.*, 2018). Finally, sugars are the primary determinant of respiration in growing tissues (Penning De Vries *et al.*, 1979; Maier *et al.*, 2010). Knowledge about whether reserves in local and connected distal tissues are used under carbon deficits and accumulated under carbon surpluses is crucial to understand carbon allocation to wood formation. Thus, experiments that directly manipulate the carbon status in the stem and monitor the effects on wood formation, metabolism and nonstructural carbon are ideally suited to improve our understanding of the sensitivity of wood formation to carbon supply.

In this study, we aim to investigate carbon fixation processes directly at the sink location in mature trees while monitoring respiration and variation in nonstructural carbon. In particular, we applied phloem girdling and reversible phloem compression to create bottlenecks restricting carbon flow along the stem (Henriksson & Rademacher, 2019). These bottlenecks can generate a large contrast in local carbon supply in stems of mature trees without affecting light, temperature, water availability, or nutrient availability for the whole tree. The resulting carbon-supply gradient is presumed to range from severe carbon limitation below the girdle, over moderate carbon limitation below the compression (due to some leakage), through moderate carbon supply surplus above the compression, to a larger increase of carbon supply above the girdle. By generating such a large local gradient in stems of mature trees within a growing season, the role of carbon supply on allocation to wood formation can be tested.

We generated such a gradient to assess the responses of wood formation and anatomy, stem respiration, and changes in nonstructural carbon concentrations and pools (soluble sugar and starch) locally and in distal needles and roots in mature *Pinus strobus* L., hereafter white pine. To differentiate between carbon supply compensation from local versus distal reserves, we added a double compression treatment that isolates a stem section from distal

nonstructural carbon reserves (Fig. 1). As a result of the induced gradient in carbon supply along the stem of mature forest trees, we hypothesise that (H1) the ratio of carbon allocation between growth, respiration and nonstructural carbon reserves will remain constant under varying carbon supply, (H2) radial wood mass growth will covary with carbon supply due to underlying correlations of carbon supply with the number of cells, cell size and cell-wall thickness of newly forming wood, (H3) stem respiration will covary with carbon supply, and finally, (H4) soluble sugar concentration will be maintained in needles, wood and roots, while starch reserves will either increase to absorb excess carbon or be depleted to supply a carbon deficit.

2. Materials and Methods

2.1 Study site - White pine at Harvard Forest

Harvard Forest is a mesic temperate mixed forest dominated by oak, maple, and pine species located in central Massachusetts, USA. Soils at Harvard Forest are derived from glacial till and characterised as well-draining, slightly acidic sandy loam with an average soil depth of one meter. Mean annual temperature at the site is 8.0 ± 0.8 ℃ ($\mu \pm \sigma$) and mean total annual precipitation is 1170 ± 193 mm ($\mu \pm \sigma$), evenly spread across all seasons (Boose & Gould, 2019).

The experiment was conducted on an even-aged cohort of white pines with homogenous growing conditions. The stand is located at 42°30.8'N and 72°13.1'W, 340 m above sea level, and is naturally regenerating since a 1990 harvest of a red pine (*Pinus resinosa* Ait.) plantation. Spacing was dense at circa. 1612 trees per hectare. For the experiment, we selected 40 healthy single-stemmed co-dominant white pines. At the beginning of the experiment, the selected trees were on average 18 ± 2 years old with a diameter at breast height of 18.7 ± 2.1 cm and a height of 10.9 ± 1.4 m ($\mu \pm \sigma$, see Table 1). The selected trees had grown on average 2.2 ± 1.2 mm y^{-1} in girth and 0.5 ± 0.1 m y^{-1} in height between 2012 and 2017 ($\mu \pm \sigma$).

2.2 Experimental setup

One of four treatments - control, single compression, double compression, or girdling - was randomly assigned to each tree, yielding ten trees per treatment. The four treatment groups had similar age, initial diameter at breast height, height, and average radial growth in the previous five years (ANOVA, p = 0.34, 0.46, 0.24, and 0.52, respectively). Dead branches below 3 m were pruned in May 2017 to facilitate access to stems.

The experiment started on the 4th of July 2017. For the control trees, no treatment was applied. For the girdling treatment, we carefully removed a 2.5 cm-wide strip of bark, phloem and cambium around the entire bole at 1.5 m stem height using razor blades (Fig. 1). We did not seal or treat the wounds. For the single compression treatment (hereafter compression treatment), collars were constructed from two ratcheted heavy-duty cargo belts with ratchets diametrically opposite each other as described in Henriksson & Rademacher (2019). Compression collars were removed after 36 days (10th of August 2017) to allow for recovery within the same growing season. For the double compression treatment, we installed identical compression belts at 1.0 m and 2.0 m stem height (Fig. 1) to isolate a stem section with regard to phloem transport to and from the canopy and the roots. Pressure below the belts was measured weekly using piezo-electric pressure sensors (Tactilus Free Form 12mm, Sensor Products Inc., Madison, New Jersey, USA). The belts generated a pressure exceeding 2 MPa around the entire circumference (Fig. S1). We re-tightened the double compression belts after 38 days (August 13th) and finally removed them after 95 days (October 10th).

2.3 Experimental monitoring

All trees were monitored during the experiment to characterise the carbon status of the trees (Fig. 1). Monitoring included a four-time characterisation of tree-ring formation and nonstructural carbon concentrations in needle, stem and root tissues, and a weekly survey of stem CO_2 efflux. Additionally, tree water status was measured weekly to evaluate potential collateral impacts (see Fig. S2 for details).

Tree-ring growth was characterised from stem microcores collected at heights shown in Fig. 1 with a Trephor (Rossi *et al.*, 2006). We collected microcores just before the experiment (July 3rd), twice during the experiment (August 8th and October 10th), and in late autumn (November 3rd). The microcores were stored in Eppendorf tubes containing a 3:1 solution of ethanol and glacial acetic acid. After 24 hours, the solution was replaced by 95% ethanol. Micro-sections (7 μm-thick cross-sectional cuts) were cut with a rotary microtome (Leica RM2245, Switzerland) from paraffin-embedded samples (Tissue Processor 1020 Leica, Switzerland) and double stained with astra-blue and safranin. Ring widths were measured using the self-developed Tree Ring Image Analysis and Database platform (http://phenocam.nau.edu/TRIAD/) on microsection images captured using a digital slide-scanner (Zeiss Axio Scan.Z1, Germany) with a resolution of roughly 1.5 pixels per μm. Tracheid anatomical characteristics (e.g., averages of lumen width and cell-wall area over 20 μm-wide tangential bands) were obtained using ROXAS 3.0.285 (von Arx & Carrer, 2014) from the November microsections.

Weekly CO_2 efflux from the stem was measured as an indicator of metabolic activity. For this purpose, chambers (10 cm diameter by 10 cm length PVC pipe) were cut to fit each tree's curvature at all sampling heights (Fig. 1) and attached two weeks prior to the treatments' start using silicone adhesive. Starting one week before the beginning of the treatments (June 29th), an infrared gas analyser (LI-820, LI-COR, Lincoln, Nebraska, USA) with a circulating pump (12K, Boxer, Ottobeuren, Germany) was attached using a PVC cap with two ports to constantly circulate air through the closed system (Carbone *et al.*, 2019). Once the concentration stabilised after closing the lid, the chamber CO_2 concentration was measured at 1 Hz for at least one minute. The raw stem CO_2 efflux and uncertainties were estimated using the RespChamberProc package (http://r-forge.r-project.org/projects/respchamberproc/) as developed by Perez-Priego *et al.* (2015).

Soluble sugar and starch concentrations in coarse roots, stems and needles were determined from tissue samples collected at the same time as the microcores (Fig. 1). Coarse roots (at least 20 cm below the root collar) and stems were cored using a 5.15 mm increment borer (Haglöf Company Group, Långsele, Sweden). Foliage samples were collected from a

sun-exposed part of the crown with a pole pruner. All sampled tissues were immediately shock-frozen on dry ice in the field and subsequently stored in a freezer (-60℃) until being cut using razor blades and freeze-dried (FreeZone 2.5, Labconco, Kansas City, Missouri, USA and Hybrid Vacuum Pump, Vaccubrand, Wertheim, Germany). Dried samples were ground by machine (mesh 20; Thomas Scientific Wiley Mill, Swedesboro, New Jersey, USA; SPEX SamplePrep 1600, MiniG, Metuchen, New Jersey, USA), although small samples were ground with pestle and mortar to minimise loss of material. An equal mix of first- and second-year needles and the entire root core were each homogenised. For stems, we homogenised the first and second centimeter of the core separately. Only July and November were analysed for the second centimeter. About 40 mg of finely ground and dried powder for all tissue, tree and sampling date combinations was analysed following the protocol by Furze *et al.* (2018). Colourimetric analysis with phenol-sulphuric acid was read twice at 490 nm for sugar and 525 nm for starch using a spectrophotometer (Thermo Fisher Scientific GENESYS 10S UV-Vis, Waltham, Massachusetts, USA), and calibrated with a 1:1:1 glucose:fructose:galactose (Sigma Chemicals, St. Louis, Missouri, USA) standard curve for sugar and a glucose (Sigma Chemicals, St. Louis, Missouri, USA) standard curve for starch. Each batch of samples included on average 35 samples, at least 10 blanks - both tube and sample blanks - and between 9 and 12 laboratory control standards (red oak stem wood, Harvard Forest, Petersham, Massachusetts, USA; potato starch, Sigma Chemicals, St. Louis, Missouri, USA). We repeated extractions for batches that showed substantial deviations in the laboratory control standards (e.g., starch recovery fraction lower than 85%). The coefficient of variation for laboratory control standards was 0.08 and 0.09 for sugar and starch concentrations in oak wood, respectively, and 0.13 for potato starch. Absorbance values for all samples were converted to concentrations in % dry weight and uncertainties with the self-developed R package NSCprocessR (https://github.com/TTRademacher/NSCprocessR).

To monitor tree water status, we measured pre-dawn needle and branch water potentials once per week per tree from the end of June to the beginning of November. Neither the two compression treatments, nor the girdling, affected tree water status (see Fig. S2 for more details).

2.4 Comparing carbon pools and fluxes in a stem section

We scaled structural growth, respiratory losses, and net changes in soluble sugars and starch reserves in the first two centimeters of wood (hereafter stem sugar and starch reserves) to a common unit of grams of carbon in a 10 cm height stem section for each experimental period (sensu Fig. 1) to directly compare the size of these carbon fluxes. For structural carbon increments we associated the cell-wall area for each 20-μm wide band with a date of formation using the fraction of the ring grown derived from the microsections (i.e., July, August, October), scaled them to the entire circumference of each stem section, multiplied them with the height of the stem section and a cell-wall density (Supplementary Information 4). For respiratory losses, we averaged weekly respiration rates for each period and scaled them to the surface of the stem sections (Supplementary Information 5). To estimate nonstructural carbon reserves, we multiplied the average soluble sugar and starch concentration in the first and second centimeter of the xylem with the volume of that tissue for each stem section, which are assumed to be a large and most easily accessible fraction of radial nonstructural carbon reserves (Richardson *et al.*, 2015; Furze *et al.*, 2020). The net change in nonstructural carbon pools for a period is the difference between each pool's size at the end and the beginning of the period (Supplementary Information 6).

2.5 Statistical analysis

We estimated treatment effects by fitting linear mixed effects models with the lme4 package (Bates *et al.*, 2015) in R v3.6.3 (R Core Team, 2019). Tree was included as a random effect to account for natural between-tree variability, and a fixed effect composed of an interaction between treatment and sampling height was added to stand in for the presumed carbon-supply gradient. When effects over time were estimated, we added date as a separate categorical fixed effect and to the treatment-sampling height interaction. Models were fitted using restricted maximum likelihood estimation. The strength and importance of estimated effects was judged in comparison with estimated variances. Hereafter, we report estimated effects ($\bar{\beta}$), their standard errors ($\bar{\sigma}$), and the *t*-value in the following format: $\bar{\beta} \pm \bar{\sigma}$ ($t = t$). All code and data to reproduce the results are currently available at https://github.com/TTRademacher/Exp2017Analysis and will be made permanently available upon publication in the Harvard Forest Data Archive.

3. Results

3.1 Changes in carbon allocation

The induced carbon-supply gradient had clear effects on growth and respiration, but not on nonstructural carbon pools (Fig. 2). The mass of new wood growth mirrored the presumed carbon-supply gradient. Substantially more carbon (20%, 86%, and 91% respectively) was sequestered in woody tissue above the compression, double compression, and girdle relative to the control over the remainder of the experiment (Fig. 2). Below both compression and double compression, growth was not discernibly affected. However, wood formation ceased completely below the girdle after roughly one month, approximately halving carbon sequestration in woody structure during the experimental period. Respiration was higher above all treatments (46% above compression, 124% above double compression, and 111% above the girdle) for the remainder of the experiment relative to the control. Stem respiration was also substantially reduced below treatments (-45% for compression, -42% for double compression, and -70% for girdling) relative to the control, even when growth was not noticeably impacted below the compression treatments (Fig. 2, 3). Over the same period, net changes in nonstructural carbon pools in the stems were more than an order of magnitude smaller than the estimated carbon fluxes to growth and respiration (Fig. 2). A detectable treatment effect on nonstructural carbon concentrations was only apparent in girdled trees.

3.2 Resulting wood characteristics

About 60.5 ± 3.4 % of the final ring width had already formed by the experimental onset, which coincided with the seasonal peak of wood growth. Control trees showed a typical progression towards smaller tracheids with thicker cell walls over the remainder of the growing season (Fig. 3) resulting in an average of 51 cells per radial file composing a 1.28 mm-wide ring for 2017.

Above the treatments, wood growth was stimulated. The final ring was on average 0.15 ± 0.18 (t = 1.90), 0.73 ± 0.18 (t = 5.24), and 0.57 ± 0.18 (t = 4.33) mm wider than the control above the compression, double compression, and girdle, respectively. Differences in ring

width could mainly be traced to changes in the number of cells that formed after treatment onset. All three treatments formed unequivocally fewer cells below the treatment versus above (10 ± 6 for compressed, 21 ± 4 for double compressed, and 27 ± 3 for girdled). Control and treated trees had similar radial cell diameters (Fig. 3). Mean cell-wall area declined slightly below treatments, which in combination with large differences in the number of cells per radial file above and below treatments caused substantial differences in cumulative cell-wall area, and hence structural biomass.

Whereas cell number increased above the treatments, marginally narrower rings (-220 ± 176 (t = -0.18) μm or -17%) with slightly thinner cell walls also formed below the girdle (Fig. 3). Relative to control, mean cell-wall area was 75 ± 29 (t = -2.55) μm^2 or 18% less below the girdle by August and 47 ± 32 (t = -1.49) μm^2 or 12% less below the compression by October. After August and October, too few cells formed below the girdle and compression to reliably quantify these trends further. Below the double compression enough cells formed to detect a pronounced decline in cell-wall area of -264 ± 35 (t = -7.48) μms^2 or 57% by November.

3.3 Alterations of stem respiration

CO_2 efflux of the control group generally declined after a peak at the start of the experiment (Fig. 4). Respiratory losses of carbon generally mirrored growth in pattern and magnitude across the gradient of carbon supply, but respiratory losses were more markedly reduced than growth below both compression treatments (Fig. 2). Treatment effects on CO_2 efflux lagged two to three weeks behind the treatment onset (Fig. 4). Over the entire treatment period the average stimulation of stem CO_2 efflux above the treatment amounted to 106%, 198%, and 143% of the control for compression, double compression, and girdling, respectively. Below the compression, double compression, and girdle, CO_2 efflux plummeted by on average 33%, 49%, and 36% of the control for the period of the treatment. Between the double compression collars, CO_2 efflux stayed close to the control (0.53 ± 0.40 (t =1.34) μmol m^{-2} s^{-1}). By November, respiration rates of both compression treatments had converged and remained indistinguishable from the control treatment for the following two growing seasons (data not shown).

3.4 Changes in nonstructural carbon reserves

Soluble sugar and starch concentrations were close to previously reported values and followed known seasonal dynamics for white pine (Furze *et al.*, 2018). Starch concentrations waned over the season with the needles displaying the largest drop. Needle, wood, and root tissues averaged soluble sugar concentrations of 8.33 ± 0.17%, 0.83 ± 0.01%, and 1.47 ± 0.05% and starch concentrations of 1.32 ± 0.14%, 0.28 ± 0.01%, and 0.31 ± 0.03% across all four measurement dates and trees, respectively.

Nonstructural carbon concentrations, in particular soluble sugars, varied little among treatments and sampling heights. In tissues above all treatments, soluble sugar concentrations mostly followed the control group (Fig. 5). Slight increases of needle soluble sugar and starch concentrations were observed in girdled trees, peaking respectively 3.30 ± 1.28% (t = 2.58) in November and roughly 1% in August and October. However, needle starch concentrations had mostly converged (0.44 ± 0.88% (t = 0.49)) with the control by November (Fig. 6). Higher needle soluble sugar concentrations were also apparent in the needles of compressed and double compressed trees, albeit even smaller than for the girdled trees, culminating in November at 0.56 ± 1.26% (t = 0.44) and 2.38 ± 1.26% (t = 1.88), respectively. Finally, wood sugar concentrations above the treatments increased marginally for the first centimeter by 0.42 ± 0.16% (t = 2.64), 0.35 ± 0.15% (t = 2.22), and 0.23 ± 0.16% (t = 1.44) for compression, double compression and girdling by November, whereas wood starch concentrations remained stable in all treatments. Changes in nonstructural carbon concentrations in the second centimeter of the wood by November were similar, but even smaller (Fig. S3).

Nonstructural carbon concentrations (in particular soluble sugar concentrations) were generally maintained under low carbon supply. Although root and wood starch concentrations had declined below the girdle by 0.65 ± 0.17% (t = -3.83) and 0.32 ± 0.07% (t = -4.48) relative to the control in November, these changes were comparatively small in relation to the seasonal variation (Fig. 6) and almost imperceptible relative to carbon sequestration in new

wood growth and carbon losses due to respiration (Fig. 2). No other tissues below the treatments were dissimilar from the control.

4. Discussion

Our observations suggest that phloem compression was successful as a reversible alternative to reduce phloem flow. Similar to Henriksson *et al.* (2015), we observed an initial divergence of respiration rates above and below compression treatments, followed by a convergence of respiration rates once compression collars were removed. The increased growth response above both compression treatments further suggests that the treatment generated an effective bottleneck for phloem transport, leading to enhanced carbon supply above the treatment. However, the similar growth below the compression treatments relative to the control without a substantial depletion of connected nonstructural carbon reserves implies that phloem flow was only reduced and not halted completely. Wood also continued to form between the double compression collars with respiration rates roughly equaling control group rates. There, too, the maintenance of growth happened without reducing the local stem nonstructural carbon reserves, indicating that some carbon continued to be transported to the cambium. The difference in respiration above versus below the double compression increased proportionally compared to the single compression, indicating that each compression zone did not completely halt phloem transport. Because phloem compression was effective, albeit somewhat leaky, phloem transport seems to have been successfully modified to generate our hypothesised carbon-supply gradient ranging from severe carbon limitation below the girdle, over moderate carbon limitation below the compression (due to some leakage) and moderate carbon supply surplus above the compression, to a larger increase of carbon supply above the girdle. Phloem transport is a mass flow. Consequently, simultaneous reduction in other phloem-transported signaling compounds, which are important for wood formation (Aloni, 2013; Buttò *et al.*, 2020), could occur and may have influenced our observed results.

Multiple studies using phloem transport manipulations have shown that stopping phloem transport can cause an early cessation or reactivation of cambial activity (Maunoury-Danger

et al., 2010; De Schepper *et al.*, 2011; Oberhuber *et al.*, 2017). However, we are not aware of studies that have shown that growth can resume in the same season following a reversible manipulation of phloem transport such as compression. Growth resumed below both compression treatments after their removal in August (single compression) and October (double compression), indicating that carbon and/or hormone availability can re-activate the cambial meristem within the same growing season. While our sampling frequency does not allow for the precise identification of critical dates of wood formation, our results suggest that cambial activity is dependent on intact phloem transport and compressed phloem tissue can recover as late as October.

Experiments like the one presented here help to understand which physiological processes may be carbon-supply limited, over which timescales, and during what time of the year. Total respiratory losses did not substantially exceed the amount of carbon sequestered by wood formation along the presumed gradient of carbon supply rate (Fig. 2). We interpret this as evidence that observed physiological responses were most likely caused by variations in carbon supply rate (and/or hormones) and not by a wound response that is independent of carbon status (Asao & Ryan, 2015). Indeed, we saw no direct evidence for a wound response, such as callus tissues or increases in the number of resin ducts.

4.1 Ratios of carbon allocation changed under varying carbon supply

Growth and respiration covaried with the presumed carbon-supply rate, but the size of nonstructural carbon pools did not, thus refuting our first hypothesis (H1), that ratios of carbon allocation to growth, respiration and nonstructural carbon reserves remain constant under varying carbon supply. Under low carbon supply, proportionally more carbon was allocated to maintain nonstructural carbon pools close to control group values, resulting in only marginal net declines in nonstructural carbon pools. A similar prioritisation of nonstructural carbon reserves was observed under low carbon supply due to defoliation (Piper *et al.*, 2015; Wiley *et al.*, 2017), drought (Hagedorn *et al.*, 2016), and low atmospheric CO_2 (Hartmann *et al.*, 2015). However, proportionally more carbon was respired and integrated into woody tissues than was added to nonstructural carbon reserves under elevated carbon supply compared to the control. This is contrasting with whole-tree effects of proportionally larger increases in

nonstructural carbon concentrations than stimulations of wood growth under elevated CO_2 (Ainsworth & Long, 2005; Körner *et al.*, 2005). Other direct phloem manipulations support our observed shift in allocation towards growth at elevated carbon supply above the girdle (Maier *et al.*, 2010; Regier *et al.*, 2010; De Schepper *et al.*, 2011; Oberhuber *et al.*, 2017). The apparent discrepancy may result from within tree feedbacks at elevated CO_2, such as non-stomatal downregulation of photosynthesis (Salmon *et al.*, 2020). Especially over several years, other factors, such as nutrients or water, could also limit wood formation pronouncedly (Norby *et al.*, 2010). Importantly, we showed that carbon consumption by wood growth and respiration are much more sensitive to variations in cambial carbon supply than nonstructural carbon pools.

4.2 Wood growth was correlated with carbon supply

Radial wood growth covaried with carbon supply. However, our hypothesis (H2) was only partially supported, because only cell division was strongly correlated with carbon supply. Both mean cell-wall area and cell size were largely unaffected by carbon supply.

The number of cells that formed after treatment onset was strongly related to the presumed carbon supply. Availability of soluble sugars is linked to cell division in plants (Smith & Stitt, 2007; Lastdrager *et al.*, 2014). Soluble sugar concentrations also influence the osmotic potential in the cambium which affects turgor pressure (Guerriero *et al.*, 2014), however we did not see an increase in soluble sugar concentrations. While carbon-supply limitation due to natural defoliation can reduce growth (Fierravanti *et al.*, 2019) and cell numbers substantially (Castagneri *et al.*, 2020), we show that cell division and to a smaller degree cell-wall deposition seem more generally regulated by carbon supply. Interestingly, the marked increase in cell number above all phloem transport manipulations also resulted in much higher cumulative cell-wall area, thus biomass, without affecting average cell size.

Contrary to previous studies, we did not see a reduction in cell-wall thickness above any of the treatments. Reduced cell-wall thickness in latewood has been reported for Norway spruce saplings above the girdle (Winkler & Oberhuber, 2017). This reduction in cell-wall deposition at higher carbon supply was attributed to either (1) additional carbon demand due to more

cells formed or (2) alternative investment in defense compounds due to a wound reaction. Winkler & Oberhuber (2017) also reported the formation of smaller lumina in earlywood above the girdle and larger lumina in latewood, in contrast to our findings of no substantial changes in cell size. Observed variations in cell-wall thickness between the two studies may be partially responsible for this difference. However, we cannot rule out that differences in phenology, especially because earlywood formation was complete by the onset of our experiment, or species may be responsible for the differing effects on cell-wall deposition and cell size. We suspect that the differences are caused by different developmental stages of the trees: saplings versus mature trees. Trees are thought to be more carbon limited at younger ages (Körner, 2003, 2006; Hayat *et al.*, 2017; Hartmann *et al.*, 2018). Importantly, we show that, instead of thickening cell-walls of normally formed cells, surplus carbon seems to trigger the proliferation of additional cells and be preferentially deposited in cell walls of those additional cells in mature trees. While carbon allocation to cell walls of normally formed versus additionally formed cells may have equivalent consequences on biomass production, they have opposing effects on water transport and safety. Therefore, it is important to further confirm this finding for other species.

4.3 Respiration co-varied with carbon supply

Stem respiration rates increased with carbon supply, supporting (H3) that the two will co-vary. Respiration rates responded within three weeks to phloem transport manipulations, but took substantially longer to relax to control group values once the compression was removed. The only other stem-compression study documented a similar effect on stem respiration, but a faster recovery after only two weeks for mature Scots pines (Henriksson *et al.*, 2015). We suspect that this discrepancy in recovery is caused due to our experiment starting later in the growing season, thus allowing only a smaller opportunity for re-growth and/or recovery of the phloem. Finally, the compression collar design used here also exerted slightly higher pressure around the circumference (Henriksson & Rademacher, 2019), which may have contributed to the longer observed recovery times.

Stem respiration declined as much below compression treatments as below girdles, despite growth remaining at control group levels below both compression treatments. Respiration

may simply be more sensitive to carbon supply. However, leaf respiration in three tropical species did not change a consequence of girdling (Asao & Ryan, 2015). Yet, the continuation of growth below the compression treatments seems to suggest that non-growth metabolism is preferentially downregulated at lower carbon supply, as evidenced in lower stem respiration. Similar respiration levels below the girdle and both compression treatments suggest that they both approached a necessary minimum, that is essential to maintain living tissue (Minchin & Lacointe, 2005). Given the lack of local depletion of nonstructural carbon reserves below treatments, we assume the carbon necessary to fuel respiration was supplied from roots reserves, more so in the girdled trees, and from leakage across the compression zone.

4.4 Wood soluble sugar and starch concentrations were stable across a large carbon-supply gradient

Soluble sugar concentrations remained remarkably constant for any individual tissue among treatments. One exception were increases in needle soluble sugar concentrations in girdled trees, which may cause non-stomatal photosynthetic down-regulation (Salmon *et al.*, 2020). Although starch concentrations buffered soluble sugar concentrations against imbalances in carbon supply and demand, as hypothesised (H4), the net fluctuations of nonstructural carbon reserves were marginal compared to fluxes due to respiration and growth. Indeed, noticeable remobilisation and accumulation of starch was only apparent in the roots and needles of girdled trees, respectively.

Previously, modelling (De Schepper & Steppe, 2011) and experimental evidence from saplings (Winkler & Oberhuber, 2017) was interpreted to suggest that an accumulation of osmotically active sugars in the cambium was responsible for observed increases in cell division due to consequent changes in turgor pressure. However, we do not see an increase in soluble sugar concentrations in the first centimeter of the xylem, despite the large increases in cell division. Soluble sugars could be a signal directly operating on cell division (Riou-Khamlichi *et al.*, 2000). Additionally, dynamic soluble sugar concentrations have already been argued to be a direct signal driving the early-to-latewood transition (Cartenì *et al.*, 2018). The observed stable soluble sugar concentrations across treatments add to a growing body of evidence that nonstructural carbon concentrations remain largely constant in

wood of mature trees (e.g., Zhang *et al.*, 2020). In fact, multiple studies did not report a detectable increase in bark and xylem sugar concentrations above phloem transport manipulations either (Regier *et al.*, 2010; Henriksson *et al.*, 2015; but see Maier *et al.*, 2010; De Schepper *et al.*, 2011). For aspen, starch mass, not concentration, was the best predictor of sprout growth, while stem sugar concentrations had no relationship with growth (Wiley *et al.*, 2019), although reduction in nonstructural carbon reserves seems to be more pronounced in mature trees (Landhäusser & Lieffers, 2012). This maintenance of soluble sugar concentrations in the cambium during the active growing season stipulates that equating high wood soluble sugar concentrations with a sink limitation (e.g. Hagedorn *et al.*, 2016) is flawed, because they seem to be regulated independently. Importantly, our results also demonstrate that we cannot simply equate soluble sugar concentrations in wood with carbon supply, as they may fulfil a direct signalling function that is essential for wood formation and helps coordinate sink-source interactions.

4.5 Conclusion

Our study has demonstrated that stem compression is a reversible way to efficiently manipulate phloem flow, which can be further harnessed to study the temporal effects of controlled phloem transport and its recovery. Compression in combination with girdling has illustrated largely stable soluble sugar concentrations along a large presumed carbon-supply gradient, whereas respiration and wood growth were both regulated by phloem transport. Concerning wood formation, cell division seems particularly sensitive to carbon supply with minor effect on cell-wall deposition. Overall, wood formation seems to be directly carbon-limited over timescales of several months. This sensitivity of wood formation to carbon supply in mature trees needs to be considered in models of the land carbon cycle.

Acknowledgements

AF, AR, and TR acknowledge support from the Natural Environment Research Council (NE/P011462/1)—National Science Foundation (DEB- 1741585) research cooperation agreement. AR is also supported by the National Science Foundation under grant DEB-1237491 and DEB-1832210. DB acknowledges support through the Swiss National

Science Foundation (PSBSP3-168701) and the Harvard Forest Bullard Fellowship. We also thank Aglaé Landry-Boisvert, Brooklynn Abaroa, Emory Ellis, Kyle Wyche, and Mark VanScoy for help in the field, Shawna Greyeyes, Amberlee Pavey, and Angelina Valenzuela for help in the lab, Katharyn Duffy, Teemu Hölttä, and Drew M. P. Peltier for feedback on the manuscript, and Henrik Hartmann, Teemu Hölttä, and Cyrille Rathgeber for friendly peer-review of the ideas and methods.

Author Contributions

TR and AR planned and designed the experiment. TR conducted the experiment, collected all data and materials. JL, MF, PF and TR conducted the laboratory analyses. BS, DB and TR created the TRIAD platform. TR developed the NSCprocessR package with input from JL and AR. TR performed the statistical analysis, generated the figures, and wrote the paper. All co-authors discussed ideas, provided feedback, edited the manuscript draft, and approved the manuscript for submission.

References

Ainsworth EA, Long SP. **2005**. What have we learned from 15 years of free-air CO_2 enrichment (FACE)? A meta-analytic review of the responses of photosynthesis, canopy properties and plant production to rising CO_2. *New Phytologist* **165**: 351–372.
Aloni R. **2013**. Role of hormones in controlling vascular differentiation and the mechanism of lateral root initiation. *Planta* **238**: 819–830.
von Arx G, Carrer M. **2014**. ROXAS – A new tool to build centuries-long tracheid-lumen chronologies in conifers. *Dendrochronologia* **32**: 290–293.
Asao S, Ryan MG. **2015**. Carbohydrate regulation of photosynthesis and respiration from branch girdling in four species of wet tropical rain forest trees. *Tree Physiology* **35**: 608–620.
Atkin O. **2015**. New Phytologist and the 'fate' of carbon in terrestrial ecosystems. *New Phytologist* **205**: 1–3.
Bates D, Mächler M, Bolker B, Walker S. **2015**. Fitting Linear Mixed-Effects Models Using lme4. *Journal of Statistical Software* **67**: 1–48.
Boose E, Gould E. **2019**. Harvard Forest Climate Data since 1964.
Buttò V, Deslauriers A, Rossi S, Rozenberg P, Shishov V, Morin H. **2020**. The role of plant hormones in tree-ring formation. *Trees* **34**: 315–335.
Cabon A, Peters RL, Fonti P, Martínez-Vilalta J, Cáceres MD. **2020**. Temperature and water potential co-limit stem cambial activity along a steep elevational gradient. *New Phytologist*.
Carbone MS, Czimczik CI, Keenan TF, Murakami PF, Pederson N, Schaberg PG, Xu X, Richardson AD. **2013**. Age, allocation and availability of nonstructural carbon in mature red

maple trees. *New Phytologist* **200**: 1145–1155.
Carbone MS, Seyednasrollah B, Rademacher TT, Basler D, Le Moine JM, Beals S, Beasley J, Greene A, Kelroy J, Richardson AD. **2019**. Flux Puppy – An open-source software application and portable system design for low-cost manual measurements of CO2 and H2O fluxes. *Agricultural and Forest Meteorology* **274**: 1–6.
Cartenì F, Deslauriers A, Rossi S, Morin H, De Micco V, Mazzoleni S, Giannino F. **2018**. The Physiological Mechanisms Behind the Earlywood-To-Latewood Transition: A Process-Based Modeling Approach. *Frontiers in Plant Science* **9**.
Castagneri D, Prendin AL, Peters RL, Carrer M, von Arx G, Fonti P. **2020**. Long-Term Impacts of Defoliator Outbreaks on Larch Xylem Structure and Tree-Ring Biomass. *Frontiers in Plant Science* **11**.
Dawes MA, Hagedorn F, Handa IT, Streit K, Ekblad A, Rixen C, Körner C, Hättenschwiler S. **2013**. An alpine treeline in a carbon dioxide-rich world: synthesis of a nine-year free-air carbon dioxide enrichment study. *Oecologia* **171**: 623–637.
De Schepper V, Steppe K. **2011**. Tree girdling responses simulated by a water and carbon transport model. *Annals of Botany* **108**: 1147–1154.
De Schepper V, Vanhaecke L, Steppe K. **2011**. Localized stem chilling alters carbon processes in the adjacent stem and in source leaves. *Tree Physiology* **31**: 1194–1203.
Deslauriers A, Huang J-G, Balducci L, Beaulieu M, Rossi S. **2016**. The Contribution of Carbon and Water in Modulating Wood Formation in Black Spruce Saplings. *Plant Physiology* **170**: 2072–2084.
Fatichi S, Leuzinger S, Körner C. **2014**. Moving beyond photosynthesis: from carbon source to sink-driven vegetation modeling. *New Phytologist* **201**: 1086–1095.
Fierravanti A, Rossi S, Kneeshaw D, De Grandpré L, Deslauriers A. **2019**. Low Non-structural Carbon Accumulation in Spring Reduces Growth and Increases Mortality in Conifers Defoliated by Spruce Budworm. *Frontiers in Forests and Global Change* **2**.
Friend AD, Eckes-Shephard AH, Fonti P, Rademacher TT, Rathgeber CBK, Richardson AD, Turton RH. **2019**. On the need to consider wood formation processes in global vegetation models and a suggested approach. *Annals of Forest Science* **76**: 49.
Fromm J. **2010**. Wood formation of trees in relation to potassium and calcium nutrition. *Tree Physiology* **30**: 1140–1147.
Furze ME, Huggett BA, Aubrecht DM, Stolz CD, Carbone MS, Richardson AD. **2018**. Whole-tree nonstructural carbohydrate storage and seasonal dynamics in five temperate species. *New Phytologist* **221**: 1466–1477.
Furze ME, Huggett BA, Chamberlain CJ, Wieringa MM, Aubrecht DM, Carbone MS, Walker JC, Xu X, Czimczik CI, Richardson AD. **2020**. Seasonal fluctuation of nonstructural carbohydrates reveals the metabolic availability of stemwood reserves in temperate trees with contrasting wood anatomy. *Tree Physiology*.
Gessler A, Grossiord C. **2019**. Coordinating supply and demand: plant carbon allocation strategy ensuring survival in the long run. *New Phytologist* **222**: 5–7.
Guerriero G, Sergeant K, Hausman J-F. **2014**. Wood biosynthesis and typologies: a molecular rhapsody. *Tree Physiology* **34**: 839–855.
Hagedorn F, Joseph J, Peter M, Luster J, Pritsch K, Geppert U, Kerner R, Molinier V, Egli S, Schaub M, *et al.*2016. Recovery of trees from drought depends on belowground sink control. *Nature Plants* **2**: 5.
Hartmann H, Adams HD, Hammond WM, Hoch G, Landhäusser SM, Wiley E, Zaehle S. **2018**. Identifying differences in carbohydrate dynamics of seedlings and mature trees to

improve carbon allocation in models for trees and forests. *Environmental and Experimental Botany* **152**: 7–18.
Hartmann H, Bahn M, Carbone M, Richardson AD. **2020**. Plant carbon allocation in a changing world – challenges and progress: introduction to a Virtual Issue on carbon allocation. *New Phytologist* **227**: 981–988.
Hartmann H, McDowell NG, Trumbore S. **2015**. Allocation to carbon storage pools in Norway spruce saplings under drought and low CO2. *Tree Physiology* **35**: 243–252.
Hartmann H, Ziegler W, Kolle O, Trumbore S. **2013**. Thirst beats hunger – declining hydration during drought prevents carbon starvation in Norway spruce saplings. *New Phytologist* **200**: 340–349.
Hayat A, Hacket-Pain AJ, Pretzsch H, Rademacher TT, Friend AD. **2017**. Modeling tree growth taking into account carbon source and sink limitations. *Frontiers in Plant Science* **8**.
Henriksson N, Rademacher TT. **2019**. Stem Compression: A Means to Reversibly Reduce Phloem Transport in Tree Stems. In: Liesche J, ed. Methods in Molecular Biology. Phloem: Methods and Protocols. New York, NY: Springer, 301–310.
Henriksson N, Tarvainen L, Lim H, Tor-Ngern P, Palmroth S, Oren R, Marshall J, Näsholm T. **2015**. Stem compression reversibly reduces phloem transport in *Pinus sylvestris* trees (D Tissue, Ed.). *Tree Physiology* **35**: 1075–1085.
Hoch G. **2005**. Fruit-bearing branchlets are carbon autonomous in mature broad-leaved temperate forest trees. *Plant, Cell and Environment* **28**: 651–659.
Hölttä T, Makinen H, Nojd P, Makela A, Nikinmaa E. **2010**. A physiological model of softwood cambial growth. *Tree Physiology* **30**: 1235–1252.
Huang J, Hammerbacher A, Weinhold A, Reichelt M, Gleixner G, Behrendt T, Dam NM van, Sala A, Gershenzon J, Trumbore S, *et al.*2019. Eyes on the future – evidence for trade-offs between growth, storage and defense in Norway spruce. *New Phytologist* **222**: 144–158.
Körner C. **2003**. Carbon limitation in trees. *Journal of Ecology* **91**: 4–17.
Körner C. **2006**. Plant CO_2 responses: an issue of definition, time and resource supply. *New Phytologist* **172**: 393–411.
Körner C, Asshoff R, Bignucolo O, Hättenschwiler S, Keel SG, Peláez-Riedl S, Pepin S, Siegwolf RTW, Zotz G. **2005**. Carbon Flux and Growth in Mature Deciduous Forest Trees Exposed to Elevated CO_2. *Science* **309**: 1360–1362.
Lamlom SH, Savidge RA. **2003**. A reassessment of carbon content in wood: variation within and between 41 North American species. *Biomass and Bioenergy* **25**: 381–388.
Landhäusser SM, Lieffers VJ. **2012**. Defoliation increases risk of carbon starvation in root systems of mature aspen. *Trees* **26**: 653–661.
Li M, Hoch G, Körner C. **2002**. Source/sink removal affects mobile carbohydrates in Pinus cembra at the Swiss treeline. *Trees* **16**: 331–337.
Maier CA, Johnsen KH, Clinton BD, Ludovici KH. **2010**. Relationships between stem CO2 efflux, substrate supply, and growth in young loblolly pine trees. *New Phytologist* **185**: 502–513.
Maunoury-Danger F, Fresneau C, Eglin T, Berveiller D, Francois C, Lelarge-Trouverie C, Damesin C. **2010**. Impact of carbohydrate supply on stem growth, wood and respired CO_2 ^{13}C: assessment by experimental girdling. *Tree Physiology* **30**: 818–830.
Minchin PEH, Lacointe A. **2005**. New understanding on phloem physiology and possible consequences for modelling long-distance carbon transport. *New Phytologist* **166**: 771–779.
Muhr J, Trumbore S, Higuchi N, Kunert N. **2018**. Living on borrowed time - Amazonian

trees use decade-old storage carbon to survive for months after complete stem girdling. *New Phytologist* **220**: 111–120.
Norby RJ, Warren JM, Iversen CM, Medlyn BE, McMurtrie RE. **2010**. CO2 enhancement of forest productivity constrained by limited nitrogen availability. *Proceedings of the National Academy of Sciences* **107**: 19368–19373.
Norby RJ, Zak DR. **2011**. Ecological Lessons from Free-Air CO_2 Enrichment (FACE) Experiments. *Annual Review of Ecology, Evolution, and Systematics* **42**: 181–203.
Oberhuber W, Gruber A, Lethaus G, Winkler A, Wieser G. **2017**. Stem girdling indicates prioritized carbon allocation to the root system at the expense of radial stem growth in Norway spruce under drought conditions. *Environmental and Experimental Botany* **138**: 109–118.
O'Brien MJ, Leuzinger S, Philipson CD, Tay J, Hector A. **2014**. Drought survival of tropical tree seedlings enhanced by non-structural carbohydrate levels. *Nature Climate Change* **4**: 710–714.
Pan Y, Birdsey RA, Fang J, Houghton R, Kauppi PE, Kurz WA, Phillips OL, Shvidenko A, Lewis SL, Canadell JG, *et al.*2011. A Large and Persistent Carbon Sink in the World's Forests. *Science* **333**: 988–993.
Penning De Vries FWT, Witlage JM, Kremer D. **1979**. Rates of Respiration and of Increase in Structural Dry Matter in Young Wheat, Ryegrass and Maize Plants in Relation to Temperature, to Water Stress and to Their Sugar Content. *Annals of Botany* **44**: 595–609.
Piper FI, Gundale MJ, Fajardo A. **2015**. Extreme defoliation reduces tree growth but not C and N storage in a winter-deciduous species. *Annals of Botany* **115**: 1093–1103.
R Core Team. **2019**. *R: A Language and Environment for Statistical Computing*. Vienna, Austria: R Foundation for Statistical Computing.
Rademacher TT, Basler D, Eckes-Shephard AH, Fonti P, Friend AD, Le Moine J, Richardson AD. **2019**. Using Direct Phloem Transport Manipulation to Advance Understanding of Carbon Dynamics in Forest Trees. *Frontiers in Forests and Global Change* **2**.
Regier N, Streb S, Zeeman SC, Frey B. **2010**. Seasonal changes in starch and sugar content of poplar (Populus deltoides x nigra cv. Dorskamp) and the impact of stem girdling on carbohydrate allocation to roots. *Tree Physiology* **30**: 979–987.
Richardson AD, Carbone MS, Huggett BA, Furze ME, Czimczik CI, Walker JC, Xu X, Schaberg PG, Murakami P. **2015**. Distribution and mixing of old and new nonstructural carbon in two temperate trees. *New Phytologist* **206**: 590–597.
Riou-Khamlichi C, Menges M, Healy JMS, Murray JAH. **2000**. Sugar Control of the Plant Cell Cycle: Differential Regulation of Arabidopsis D-Type Cyclin Gene Expression. *Molecular and Cellular Biology* **20**: 4513–4521.
Rossi S, Anfodillo T, Menardi R. **2006**. Trephor: A New Tool for Sampling Microcores from tree stems. *IAWA Journal*: 89–97.
Rossi S, Simard S, Deslauriers A, Morin H. **2009**. Wood formation in Abies balsamea seedlings subjected to artificial defoliation. *Tree Physiology* **29**: 551–558.
Salmon Y, Lintunen A, Dayet A, Chan T, Dewar R, Vesala T, Hölttä T. **2020**. Leaf carbon and water status control stomatal and nonstomatal limitations of photosynthesis in trees. *New Phytologist* **226**: 690–703.
Schmid S, Palacio S, Hoch G. **2017**. Growth reduction after defoliation is independent of CO2 supply in deciduous and evergreen young oaks. *New Phytologist* **214**: 1479–1490.
van der Sleen P, Groenendijk P, Vlam M, Anten NPR, Boom A, Bongers F, Pons TL, Terburg G, Zuidema PA. **2015**. No growth stimulation of tropical trees by 150 years of CO2

fertilization but water-use efficiency increased. *Nature Geoscience* **8**: 24–28.
Vieira J, Carvalho A, Campelo F. **2020**. Tree Growth Under Climate Change: Evidence From Xylogenesis Timings and Kinetics. *Frontiers in Plant Science* **11**.
Voelker SL, Muzika R-M, Guyette RP, Stambaugh MC. **2006**. HISTORICAL CO_2 GROWTH ENHANCEMENT DECLINES WITH AGE IN *QUERCUS* AND *PINUS*. *Ecological Monographs* **76**: 549–564.
Weber R, Gessler A, Hoch G. **2019**. High carbon storage in carbon-limited trees. *New Phytologist* **222**: 171–182.
Wiley E, Casper BB, Helliker BR. **2017**. Recovery following defoliation involves shifts in allocation that favour storage and reproduction over radial growth in black oak. *Journal of Ecology* **105**: 412–424.
Wiley E, Huepenbecker S, Casper BB, Helliker BR. **2013**. The effects of defoliation on carbon allocation: can carbon limitation reduce growth in favour of storage? *Tree Physiology* **33**: 1216–1228.
Winkler A, Oberhuber W. **2017**. Cambial response of Norway spruce to modified carbon availability by phloem girdling. *Tree Physiology* **37**: 1527–1535.
Zhang P, Zhou X, Fu Y, Shao J, Zhou L, Li S, Zhou G, Hu Z, Hu J, Bai SH, *et al.*2020. Differential effects of drought on nonstructural carbohydrate storage in seedlings and mature trees of four species in a subtropical forest. *Forest Ecology and Management* **469**: 118159.

Tables

Table 1: Summary statistics for the treatment groups including mean diameter at 1.5 m above the root collar, mean height ($\mu \pm 1\sigma$ for both), start and end date and duration.

treatment	n	dbh (cm)	h (m)	start	end	duration (days)
control	10	18.2 ± 1.5	10.7 ± 1.6	-	-	-
girdled	10	18.9 ± 2.2	11.1 ± 1.5	4th July	-	-
compressed	10	18.2 ± 2.0	11.4 ± 0.7	4th July	10th August	36 days
double compressed	10	19.7 ± 2.4	10.5 ± 1.7	5th July	10th October	95 days

Figures

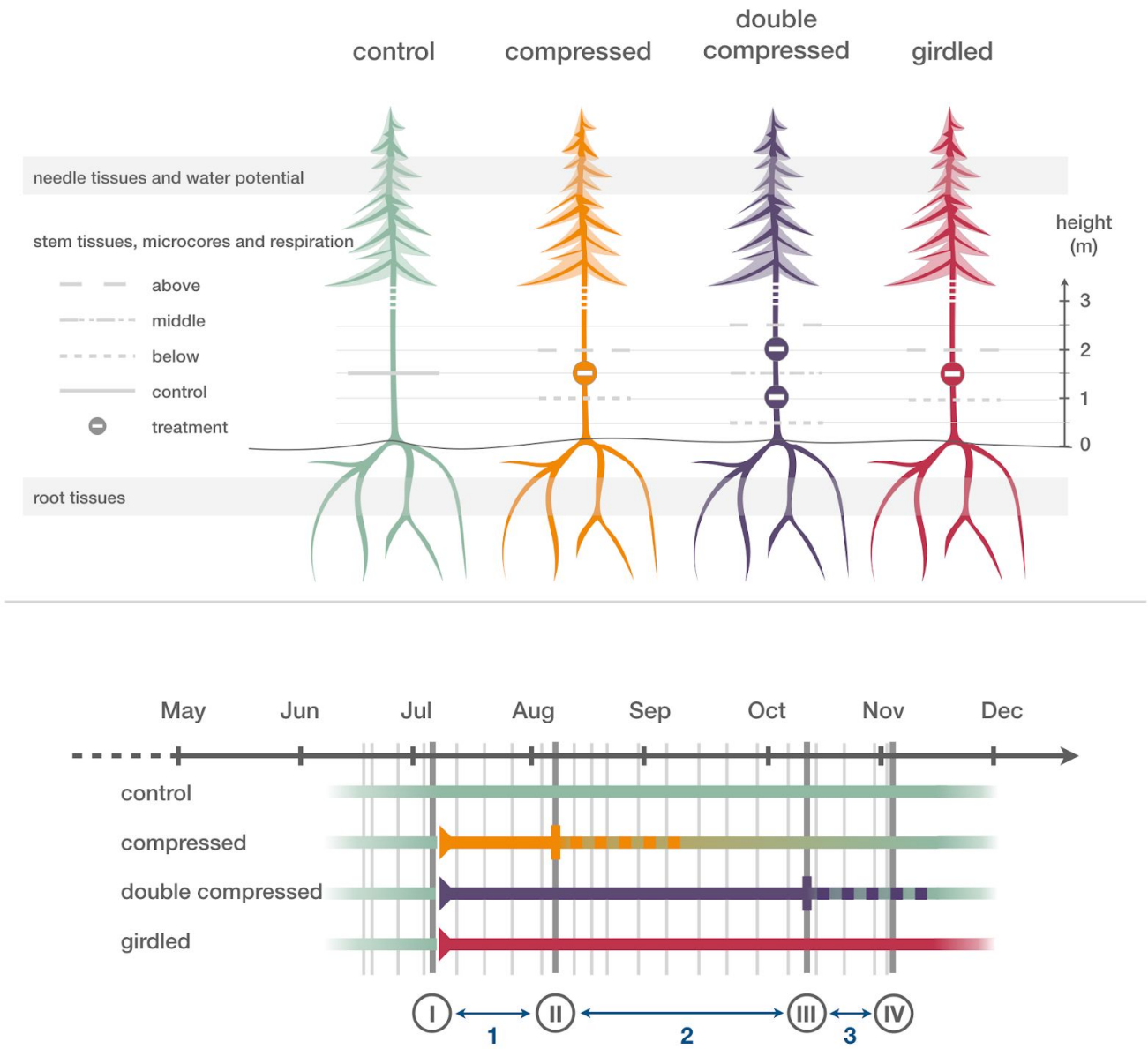

Figure 1 - Experimental setup (top panel) and timeline (bottom panel). For all treated trees, stem measurements of respiration, microcores and stem tissue samples were taken 0.5 m above (dashed lines) and below (dotted lines) the respective treatment. For double compressed trees, a third measurement in the middle of the two compression collars (dash-dotted line) was taken. For the control trees, one measurement (solid line) was taken at 1.5 m above the root collar. Additionally, root and needle tissue samples were collected. The experiment started in early July with baseline measurements directly followed by the experimental onset. Four dates of intensive sampling (I, II, III, and IV) are indicated by thick, vertical, dark grey bars. On these sampling dates microcores and tissue samples for needles, stem wood and roots were collected. These dates divide the experiment into

three distinct periods (1, 2, 3). Stem respiration and water potential of needles and branches was measured weekly as indicated by the thinner, light grey, vertical bars.

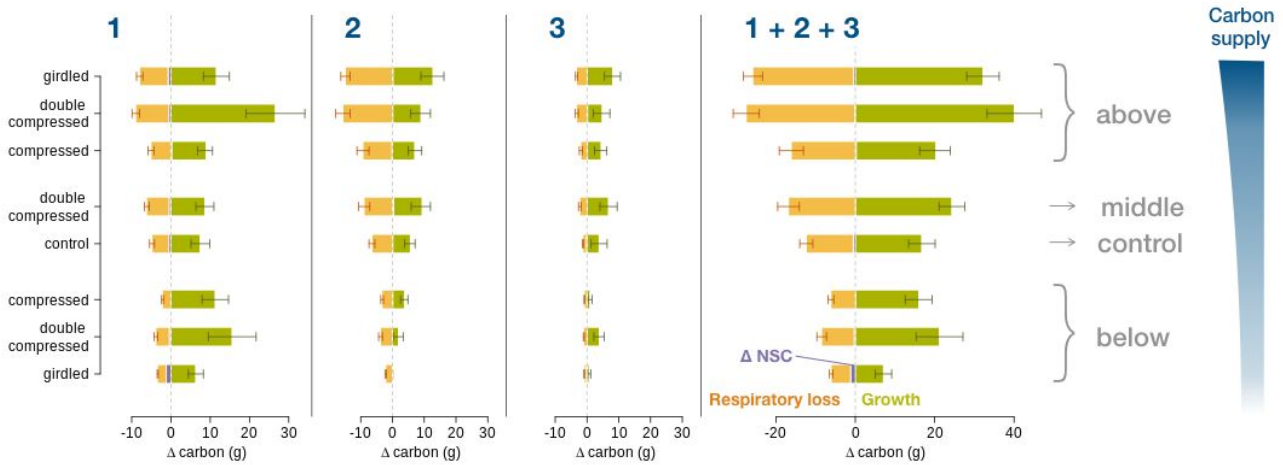

Figure 2 - Carbon budget (integral of growth, respiratory losses and net change in nonstructural carbon pools in the first centimeter) for an average 10 cm-high stem section over three periods. Sections are sorted along a presumed carbon-supply gradient from highest above the girdle to lowest below the girdle illustrated schematically on the right. The panel numbers correspond to the periods indicated in the timeline (Fig. 1): (1) first month of the experiment, (2) second and third month after experimental onset, and (3) fourth month after experimental onset. The panel (1+2+3) shows the cumulative changes from the beginning of July to November. Respiratory losses (orange), radial mass growth (green), and net changes in total nonstructural carbon pools in the first centimeter (purple) are shown for each treatment and sampling height (A = above, B = below, M = middle, and C = control). Error bars indicate one standard error. For details on the scaling assumptions of structural carbon, respiration, and nonstructural carbon see Supplementary Information 4, 5, and 6, respectively.

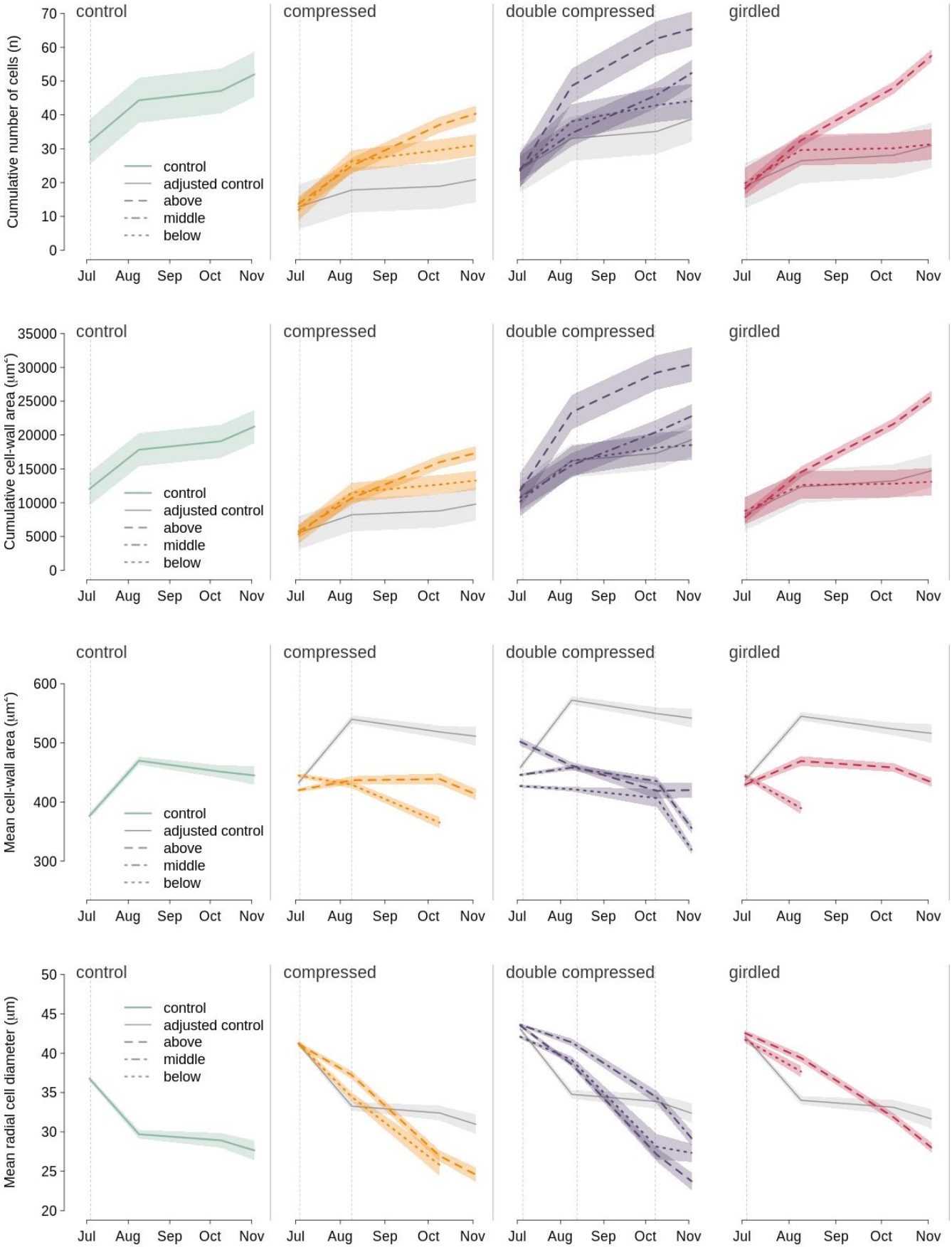
control
compressed
double compressed
girdled
Cumulative number of cells (n)
Cumulative cell-wall area (µm²)
Mean cell-wall area (µm²)
Mean radial cell diameter (µm)
control
adjusted control
above
middle
below
Jul
Aug
Sep
Oct
Nov

Figure 3 - Treatment effects on wood formation and the resulting anatomy in stem sections of control trees (solid line), as well as above (dashed lines), in the middle of (dash-dotted line) and below (dotted line) treatment zones of treated trees over time. For stem sections from control (left column; green), compressed (second column; orange), double-compressed (third column; purple) and girdled trees (right column; red), we show the cumulative number of cells (top row), the cumulative cell-wall area (second row), mean cell-wall area per cell (third row), and mean radial cell diameter (fourth row). Lines and shading indicate the mean and one standard error and are coloured by treatment. Means are not displayed when the average period growth did not exceed 0.05 mm ($n < 25$ 20-μm wide zones). For ease of comparison, the control group is normalised with respect to the treatment's July baseline and displayed in grey. Dashed grey vertical lines indicate key dates for each treatment, such as start date, re-tightening date and end date.

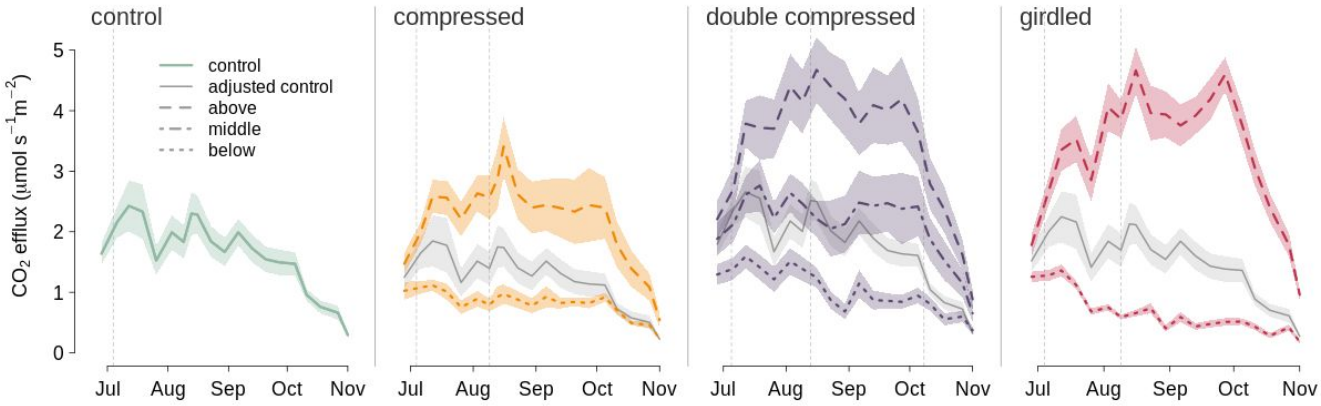

Fig. 4 - Mean stem CO_2 efflux (line) and one standard error (shading) by treatment (colour) and sampling height (line type) over time. For reference, the control group mean and standard error are normalised to the treatment baselines and plotted in grey in the background for all other treatments. The grey vertical dashed lines mark the appropriate key dates for each treatment, such as start date, re-tightening date and end date.

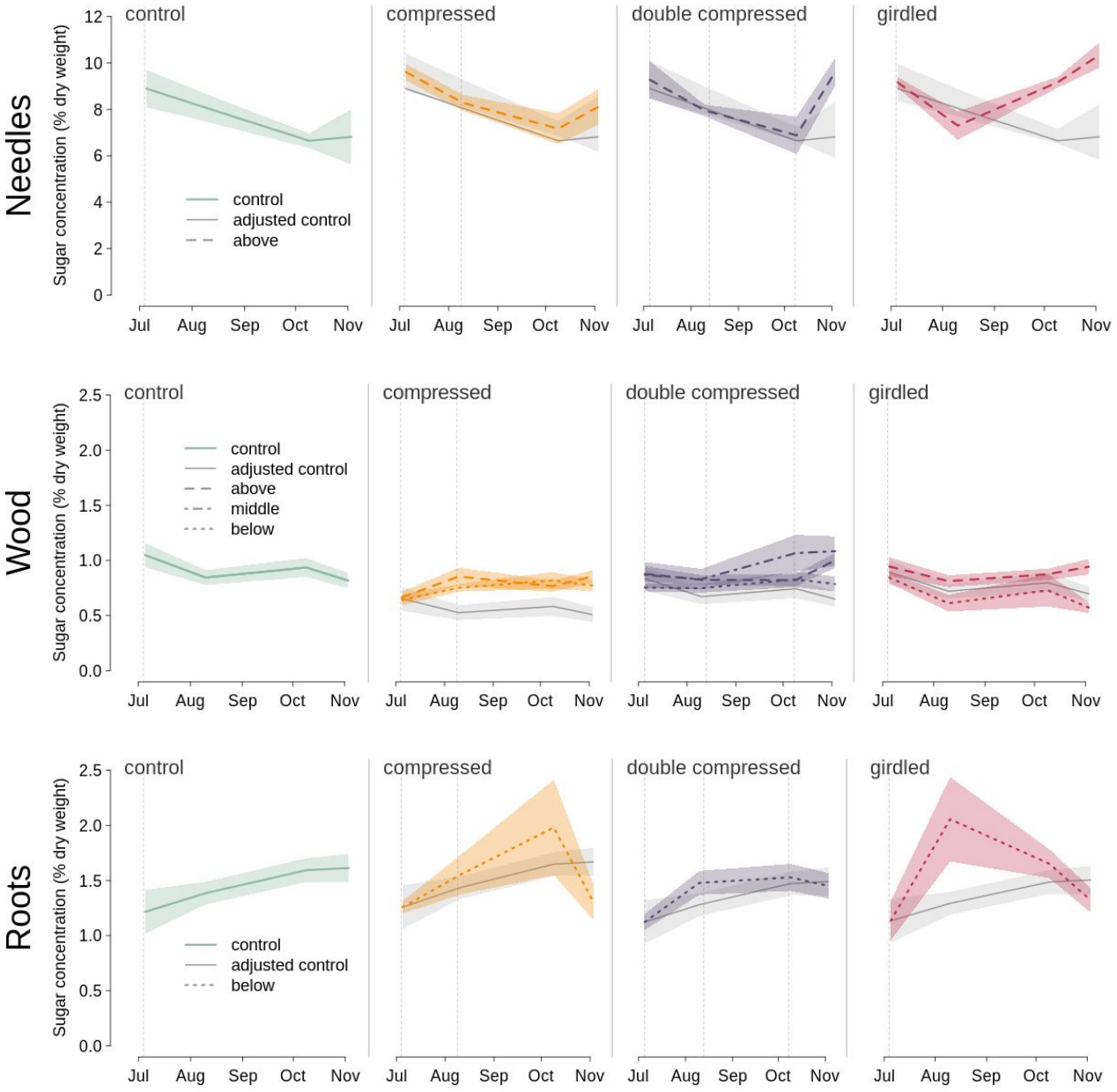

Fig. 5 - Soluble sugar concentrations in needles (top row), the first centimetre of the xylem (middle row), and coarse roots (bottom row) for the control (left column; green), compressed (second column; orange), double-compressed (third column; purple), and girdled (right column; red) trees over time. Coloured lines and shading show the mean and one standard error with colours corresponding to the treatment. Line type corresponds to the spatial positioning relative to the treatment with solid lines for control, dashed lines for above the treatment, dotted lines for below, and dash-dotted lines for in the middle of two treatment zones. For ease of comparison, the control group is adjusted for baseline differences and added to all treatment panels (grey line and shading). Key dates - start and end date as well as date of re-tightening of compression bands - are indicated by grey, dashed vertical lines.

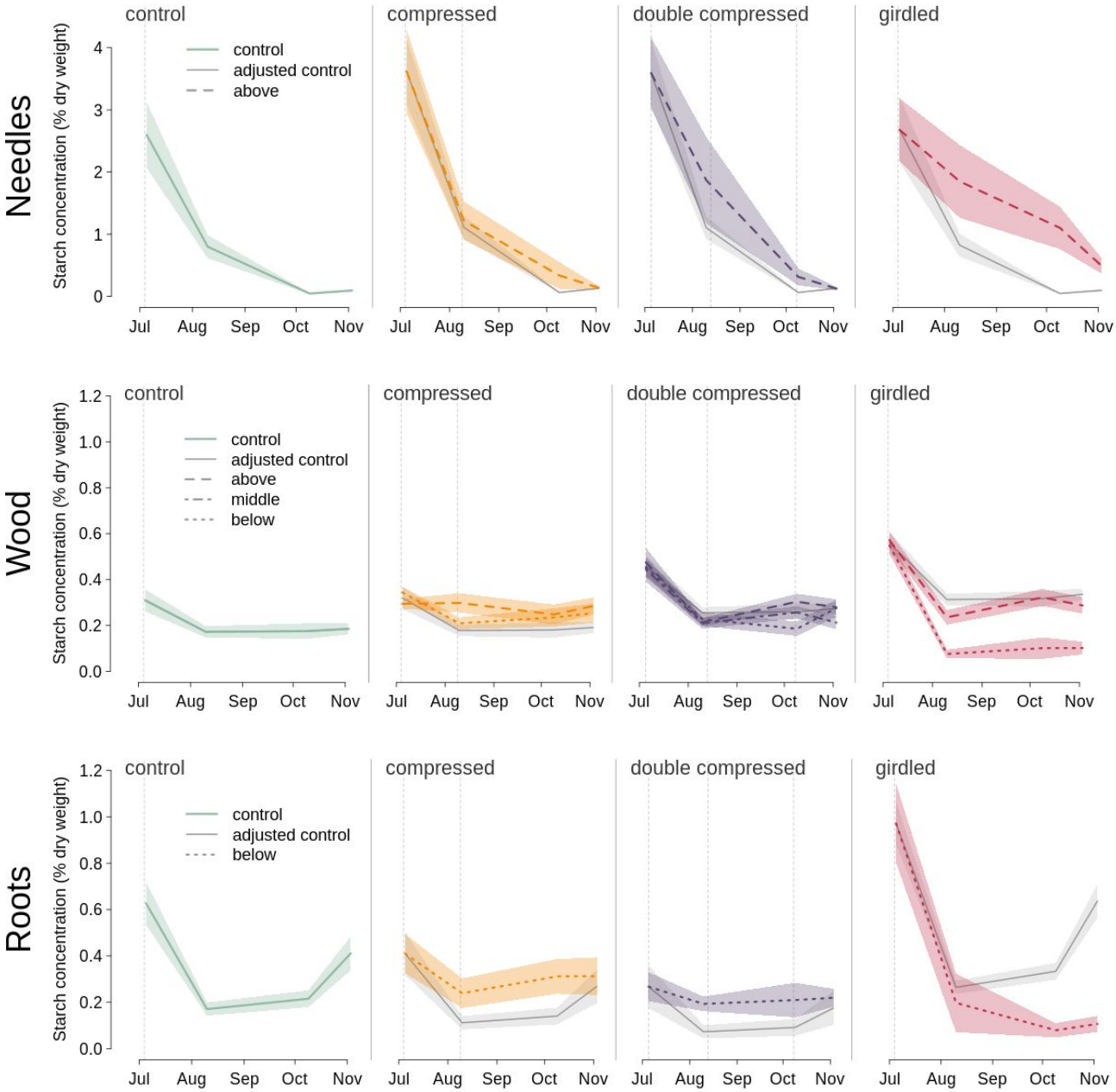

Fig. 6 - Starch concentrations in needles (top row), the first centimeter of the xylem (middle row), and coarse roots (bottom row) for the control (left column; green), girdled (second column; orange), compressed (third column; purple), and double compressed (right column; red) trees over time. Coloured lines and shading show the mean and one standard error with colours corresponding to the treatment. Line type corresponds to the spatial positioning relative to the treatment with solid lines for control, dashed lines for above the treatment, dotted lines for below, and dash-dotted lines for in the middle of two treatment zones. For ease of comparison, the control group is adjusted for baseline differences and added to all treatment panels (grey line and shading). Key dates - start and end date as well as date of re-tightening - are indicated by grey, dashed vertical lines.

Supporting Information

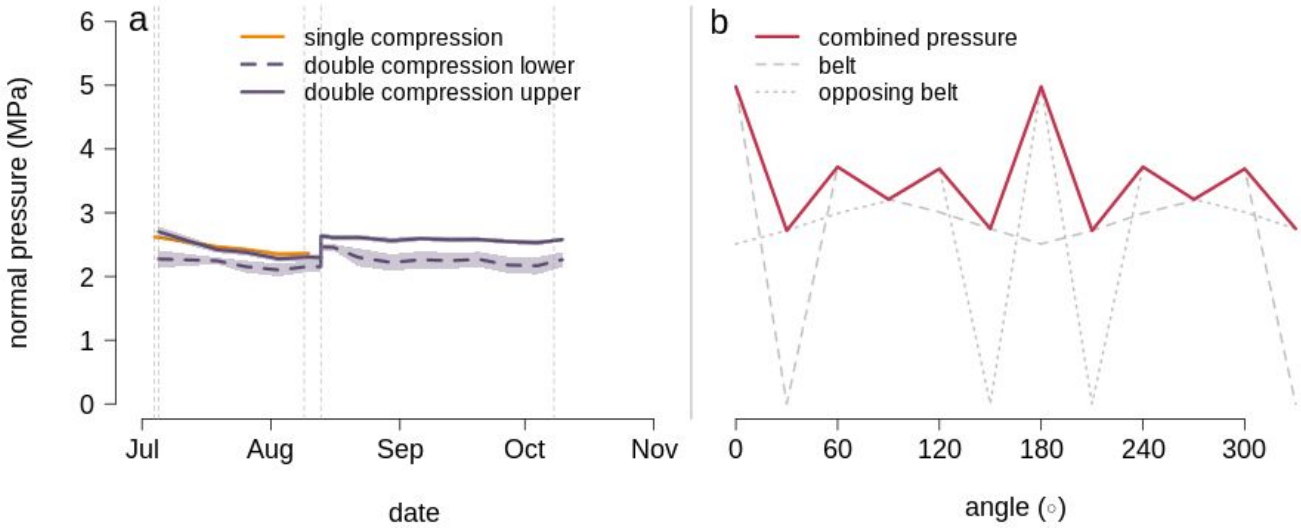

Fig. S1 - (a) Mean collar pressure and one standard deviation (shading) over time for the single (orange) and double compression (purple) treatments. Key dates (e.g., start, re-tightening and end) are indicated by the grey dashed vertical lines. (b) Circumferential pressure distribution as measured in the lab before deployment using piezo-electric pressure sensors. The dashed and dotted lines show the pressure exerted by an individual compression belt, and the red line the combined pressure of two diametrically opposing belts.

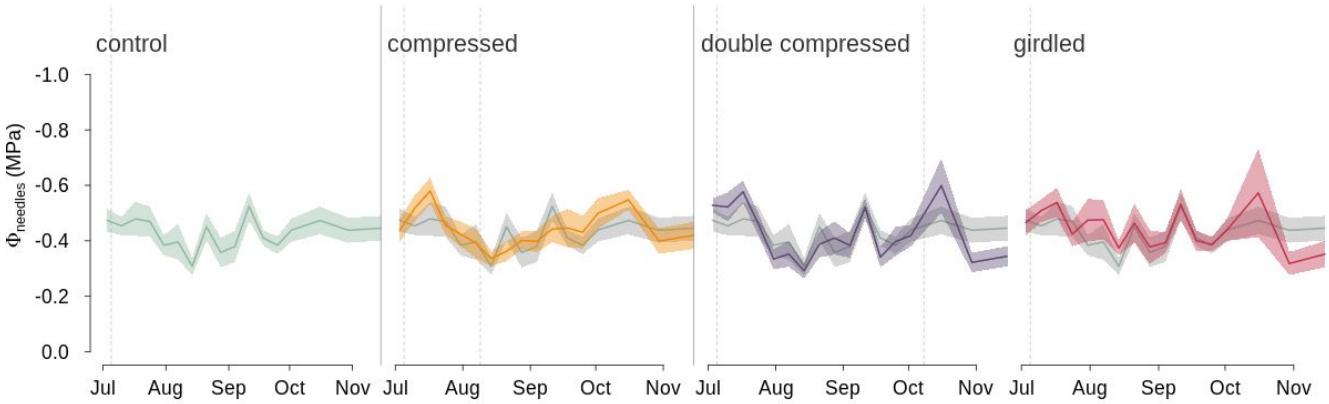

Fig. S2 - Weekly mean (solid line) and one standard error (shading) of needle water potential ($\Phi_{needles}$) for the control, compressed, double-compressed, and girdled trees. The control group mean and standard error are shown on treatment panels in grey to facilitate comparison. Key dates for each treatment (e.g., start, re-tightening and end date) are indicated by dashed grey vertical lines. Pre-dawn needle and branch water potential were measured with a pressure chamber (Model 600, PMS Instruments, Albany, Oregon, USA) once per week per tree from the end of June to the beginning of November (displayed above) and twice in the two following years (not shown).

For each measurement, two branch tips per tree were cut, sealed in air-tight plastic bags for transport. Initial tests showed that water potential could be determined accurately up to 20 minutes after cutting the tissue. Within 20 minutes of harvest, water potential was determined after re-cutting the tissue. Observed needle and branch water potential did not differ among treatments during the duration of the experiment or in the remaining growing season.

After about one year, the girdled trees had substantially more negative needle water potentials (not shown), from -046 ± 0.06 MPa to -0.91 ±0.08 MPa (5.20). All girdled trees showed clear signs of decline, such as canopy browning, and seven trees died about two years after the girdling (2019). With the exception of one compressed tree, which died in 2018, neither the single nor the double compression had a detectable effect on pre-dawn water potentials for the two following growing seasons.

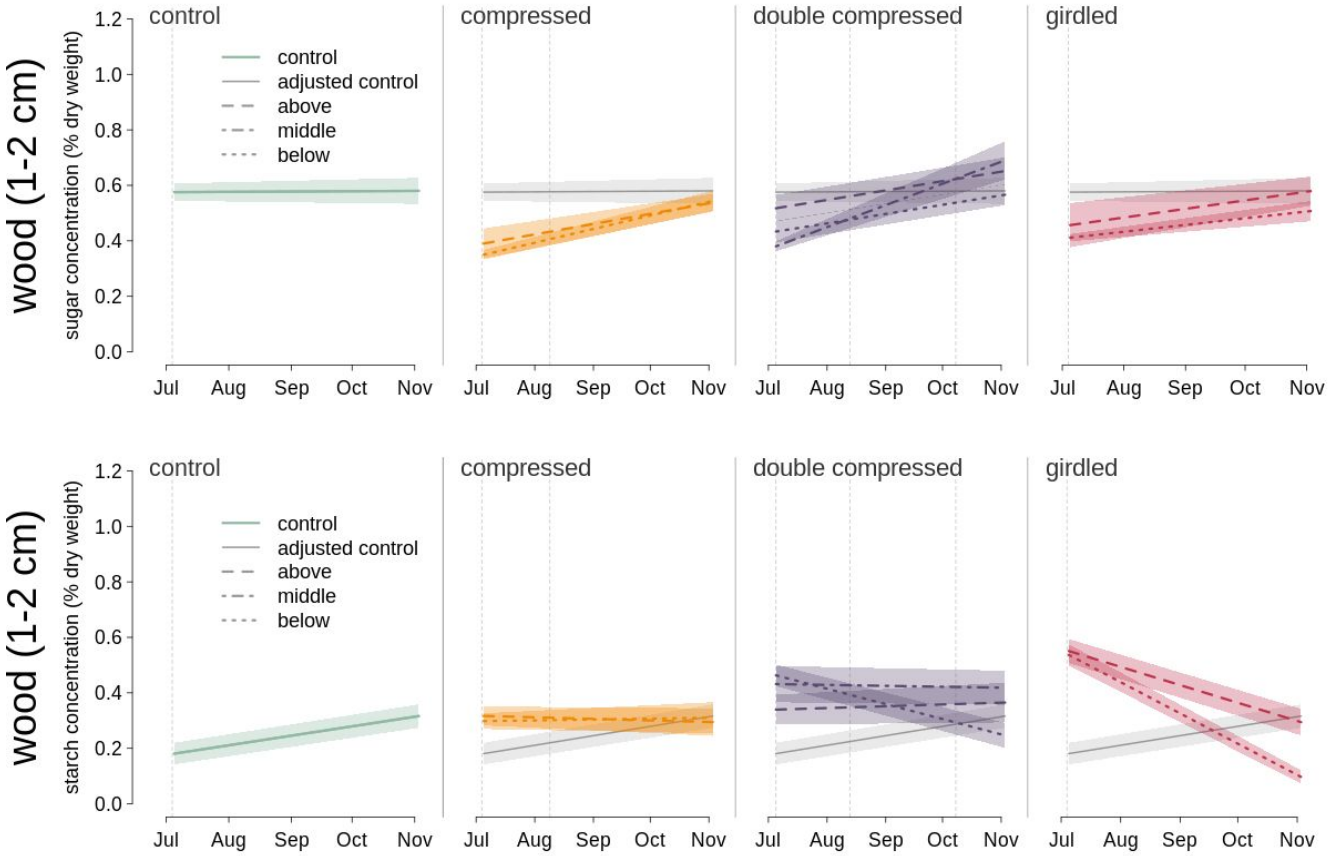

Fig. S3 - Soluble sugar (top row) and starch concentrations (bottom row) in the second centimeter (e.g., 1 to 2 cm range) of the wood for the control (left column; green), compressed (second column from the left; orange), double compressed (second column from the right; purple), and girdled trees (right column; red). The lines indicate the mean concentration with shading representing one standard error. For ease of comparison, control values were added to all treatment panels in grey. Key dates for each treatment (e.g., start, re-tightening and end date) are indicated by dashed grey vertical lines. Dashed lines correspond to tissues above the treatment, dotted line to tissue below the treatment and dashed-dotted lines to tissues in the middle of the double compression.

The changes in concentrations from July to November were less than in the first centimeter (t-test, $p = 0.007341$ for sugar and $p = 0.000426$ for starch).